Numerical Analysis of Thermal Management System for Li-Ion Batteries: A Multiscale Modeling Technique

Talal Bin Irshad[*1], Abid Hussain[1]

[1]Department of Mechanical Engineering, University of Engineering and Technology, Taxila, Pakistan

[*]talalbinirshad@gmail.com

Abstract:

Electric vehicles mainly depend on Li-ion batteries. Temperature beyond a permissible range is caused by the rapid charging and discharging of high-power Li-ion batteries. Because of the high thermal efficiency, Passive cooling using Phase Change Material is the most effective cooling methods. In this study, the 1D Li-ion battery model attached to a 3D heat transfer model using a heat generating variable is studied using the Multiscale modelling technique. Numerical analysis is done by simulating the battery pack by using computational fluid dynamic software COMSOL Multiphysics 5.5. The behavior of battery pack's temperature is investigated at various C-rates. The outcome clearly suggests that adding nickel foam to the battery pack enhances temperature control. Nickel paraffin composite temperature is about 31% lower than that of natural air circulation. The pure PCM also reduces the temperature by 23% when compared to natural air circulation.

Keywords:

Li-Ion Battery, Metal foam, Thermal Management, Numerical Analysis Phase Change Material,

Introduction:

A wide range of applications uses Li-ion batteries, ranging from remote controls to electric vehicles, due to their high energy density and extended life. High operating temperatures when charging and discharging endanger the safety and durability of Li-ion batteries. The battery's operating temperature should not exceed 60°C [1]. To increase the performance and life span of Battery Thermal Management System (BTMS), several cooling techniques are offered. The first involves internal alterations such as changing chemicals compositions and materials, while the second involves eliminating heat from the battery externally. Currently, the external thermal management system has been mainly focused on. The external thermal management system is divided into two parts: active cooling, which mostly uses air convection, and latent heat thermal storage, which uses PCM to attain the appropriate battery temperature because PCM can store a large amount of heat. [3]. Using PCM, Lazrak et al. [4] attempted to make the temperature distribution inside a lithium-ion battery pack and its cells as uniform as possible. After the phase change process inside the PCM was finished, computational and experimental results showed that the new system was more effective at lowering the system temperature. Samimi et al. [5] investigated the thermal performance within the PCM by evaluating the effect of carbon fibre loading. Some authors suggested that using metal foam with PCM can enhance the thermal conductivity of PCM up to 70 W/m.K [6][7][8].

In the current numerical analysis, the electrochemical reactions and heat generation were computed using Newman's pseudo-2D electrochemical model [9]. The coupling technique used in current work was studied by Bohayra et al. [10] using COMSOL Multiphysics.

Numerical Modeling:

Figure 1 depicts the numerical model used in this research. Newman's pseudo-2D electrochemical model [9] was used to drive the model used in this study to model Li-ion batteries at various C-Rates. To simulate battery performance, a one-dimensional (1D) model presents the three-dimensional (3D) structure as shown in Fig 1. During battery discharge at various C-Rates, the electrochemical processes inside the battery were leveraged to achieve reversible and irreversible volumetric heat generation. The major purpose of the electrochemical model was to figure out how much heat was generated inside the battery at different C-Rates. The heat generated was then used to investigate the temperature rise in the battery pack with a 3D heat transfer model.

The battery pack's 3D model, as illustrated in Figure 1, 1b, consists of six embedded Li-ion batteries in either PCM-metal foam composite or PCM. The diameter and height of each battery are 18.4mm and 65mm, respectively, based on the Panasonic NRC18650B commercial cell with a capacity of 3.4Ah. The thermal conductivity of each cell is 3.3 W/m K, while the heat capacity is 1300 J/g K, and the density is 2500 kg/m^3. [11].

Electrochemical Model:

The positive anode, the electron-impeding separator, and the negative cathode filled with electrolyte make up the basic Li-ion battery as presented in Figure 1. Based on the 2D Newman's pseudo model, four coupling partial differential equations (PDE) were solved to determine the performance of the Li-ion cell. The time evolution and potentials of the lithium (Li) focus profile undergo charge conversation inside the electrode and electrolyte. The differential equations are addressed as a 1D issue in the numerical model to simulate the solid particles that contain Li atom transport. The positive and negative electrodes in the following experiment are composed of Graphite (Li_yC_6), Meso carbon micro bead (MCMB) and LMO ($Li_xMn_2O_4$), respectively. $LiPF_6$ is used as an electrolyte. The reactions for two electrodes are written as

$$Li_{y-x}Mn_2O_4 + xLi^+ + xe^- \overset{Charge}{\rightarrow} Li_yMn_2O_4 \quad (1)$$

$$Li_xC_6 \overset{discharge}{\rightarrow} LiC_6 + xLi^+ + xe^- \quad (2)$$

Newman's pseudo-2D model is commonly applied to Li-ion battery modelling [12][13], the differentials equations and boundary conditions are briefed in Table 1. Bruggeman's relation [14] was used to acquire the effective properties.

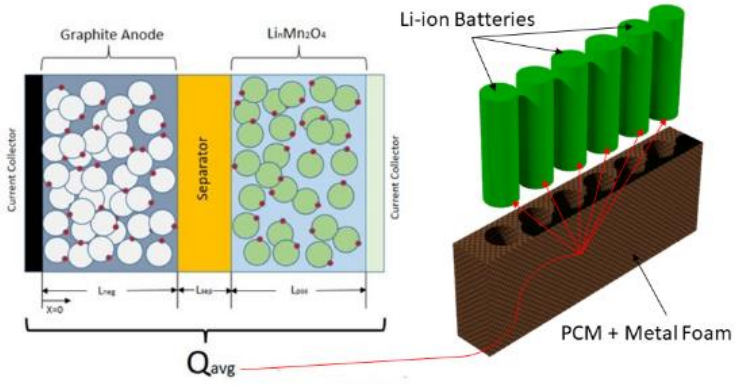

Figure 1. Illustration Of Model Developed in This Study (a) Electrochemical Model (b) 3D Heat Transfer Model

Table 1 - Boundary Conditions and Governing Equations as per Newman's pseudo-2D model and Bergman's relation [10]

Electrochemical Equation		Boundary Condition
Mass balance (Electrolyte phase)	$\frac{\partial(\varepsilon_e c_e)}{\partial t} = \frac{\partial}{\partial x}\left(D_e^{eff}\frac{\partial}{\partial x}C_e\right) + \frac{1+t_+^0}{F}j^{Li}$	$\frac{\partial c_e}{\partial x}\|_{x=0} = \frac{\partial c_e}{\partial x}\|_{x=L_n+L_{sep}+L_p} = 0$
Mass balance (Solid-phase)	$\frac{\partial c_s}{\partial t} = \frac{D_s}{r^2}\frac{\partial}{\partial r}\left(r^2\frac{\partial c_s}{\partial r}\right)$	$\frac{\partial c_s}{\partial r}\|_{r=0} = 0, -D_s\frac{\partial c_s}{\partial r}\|_{r=R_s} = \frac{j^{Li}}{a_s F}$
Electric potential (Electrolyte phase)	$\frac{\partial}{\partial x}\left(k^{eff}\frac{\partial}{\partial x}\varphi_e\right) + \frac{\partial}{\partial x}\left(k_D^{eff}\frac{\partial}{\partial x}lnc_e\right) + j^{Li} = 0$	$\frac{\partial \varphi_e}{\partial x}\|_{x=0} = \frac{\partial \varphi_e}{\partial x}\|_{x=L_n+L_{sep}+L_p} = 0$
Electric potential (Solid-phase)	$\frac{\partial}{\partial x}\left(\sigma^{eff}\frac{\partial}{\partial x}\varphi_s\right) = j^{Li}$	$-\sigma_n^{eff}\frac{\partial \varphi_s}{\partial x}\|_{x=0} = \sigma_p^{eff}\frac{\partial \varphi_e}{\partial x}\|_{x=L_n+L_{sep}+L_p} = \frac{I}{A}\frac{\partial \varphi_s}{\partial x}\|_{x=L_n} = \frac{\partial \varphi_s}{\partial x}\|_{x=L_n+L_s} = 0$
Effective properties		
Electrolyte ionic conductivity		$k^{eff} = D_e\varepsilon_e^{burg}$
Solid-phase electronic conductivity		$\sigma^{eff} = \varepsilon_s\sigma$
Electrolyte ionic diffusion conductivity		$k_D^{eff} = \frac{2RTk^{eff}}{F}(1-t_+^0)$
Electrolyte ionic diffusivity		$D_e^{eff} = D_e\varepsilon_e^{burg}$

The interface between the active particles and the electrolyte's charge transfer rate was simulated using the Butler-volume equation [9]:

$$j^{ii} = a_s i_0 \left\{ exp\left[\frac{0.5F}{RT}\eta\right] - exp\left[-\frac{0.5F}{RT}\eta\right]\right\} \quad (3)$$

The electrochemical 1D model has three line segments among which one is positive electrode, second is negative electrode with a third separator, was solved using COMSOL.

$$Q_h = comp1.aveop1(comp1.liion.Q_h) \cdot \frac{(L_{neg}+L_{sep}+L_{pos})}{L_{batt}} \quad (4)$$

Where, Q_h represents the heat generated in the li-ion battery model.

Table 2 - Electrochemical parameters for Li-ion battery model [12][16][17]

Parameter	Description	Positive electrode	Separator	Negative electrode
$б$	Solid phase conductivity	10		100
L	Electrode's length (μm)	70	25	73.5
ε_s	Volume fraction of solid phase	0.55	-	0.50
K_i	Coefficient of reaction rate (A $m^{2.5}/mol^{1.5}$)	$6.67x10^{-11}$	-	$1.764x10^{-11}$
ε_e	Electrolyte phase volume fraction	0.30	0.45	0.44
$C_{s,\,max}$	Solid phase's max. concentration (mol/m^3)	49943	-	31858
ε_b	Binder volume fraction	0.15	-	0.0566
r	Radius of solid particle (μm)	8.5	-	12.5
t^0	Transfer number of electrolyte	0.363	0.363	0.363
$C_{e,0}$	Electrolyte's initial concentration (mol/m^3)	2000	2000	2000
D_s	Coefficient of solid phase diffusion (m^2/s)	$10x10^{-14}$	-	$3.89x10^{-14}$
$brug$	Bruggeman coefficient	1.5	2.3	4.1

Heat Transfer Model:

A three-dimensional heat transfer model with six Li-ion batteries inside a solid domain that acts as either PCM or PCM-Metal foam composite is presented in Fig.1. b. Cells have a radius of 18.4mm and a height of 65mm. The PCM/PCM-metal foam composite domain has dimensions of 165mm x 25mm x 65mm, and the cells are inserted inside at 18.3mm to produce a 6s battery pack.

Based on our research [18], the PCM employed in this investigation is Rubitherm 42. Table 3 lists the characteristics of PCM and metal foam.

Table. 3.

Properties of PCM and Nickle foam

Property	Nickle Foam [19]	PCM [20]
Density (solid) (kg/m^3)	8900	880
Density (liquid) (kg/m^3)		760
Heat Capacity (J/K)		2000
Thermal expansion coefficient (1/K)		0.0005
Thermal conductivity (solid) (W/(mK))	90	0.2
Melting temperature (°C)	1450	38-41
Latent heat (J/kg)		165
Thermal conductivity (liquid) (W/(mK))		0.2

Governing equations:

The method implied to simulate phase-change material composed of continuous, momentum and energy equations.

Continuity equation:

$$\frac{\partial \rho}{\partial t} + \frac{\partial(\rho u)}{\partial x} + \frac{\partial(\rho v)}{\partial y} + \frac{\partial(\rho w)}{\partial z} = 0 \quad (5)$$

The above equation represents time as t and u, v, and w presents the direction towards x, y, and z plane. PCM begins to melt during the heating phase, and the flow process can be predicted using the momentum equation:

$$\frac{\rho_p}{\varepsilon}\frac{\partial u}{\partial t} + \frac{\rho_p}{\varepsilon^2}(V^{\rightarrow}\triangle^{\rightarrow}).u = -\frac{\partial p}{\partial x} + \frac{\mu}{\varepsilon}(\triangle^2 u) - \left(\frac{\mu}{K} + \frac{\rho_p C}{\sqrt{k}}|u|\right)u + S_u \quad (6)$$

$$\frac{\rho_p}{\varepsilon}\frac{\partial v}{\partial t} + \frac{\rho_p}{\varepsilon^2}(V^{\rightarrow}\triangle^{\rightarrow}).v = -\frac{\partial p}{\partial y} + \frac{\mu}{\varepsilon}(\triangle^2 v) - \left(\frac{\mu}{K} + \frac{\rho_p C}{\sqrt{k}}|v|\right)v + S_v \quad (7)$$

$$\frac{\rho_p}{\varepsilon}\frac{\partial w}{\partial t} + \frac{\rho_p}{\varepsilon^2}(V^{\rightarrow}\triangle^{\rightarrow}).w = -\frac{\partial p}{\partial z} + \frac{\mu}{\varepsilon}(\triangle^2 w) - \left(\frac{\mu}{K} + \frac{\rho_p C}{\sqrt{k}}|w|\right)w + S_w \quad (8)$$

$$S_u = \frac{(1-\theta)^2}{(\theta^3+\psi)}A_m u \quad (9), \qquad S_v = \frac{(1-\theta)^2}{(\theta^3+\psi)}A_m v + \rho_p g\beta\left(T - T_{ref}\right) \quad (10), \qquad S_z = \frac{(1-\theta)^2}{(\theta^3+\psi)}A_m w \quad (11)$$

According to Volter and Prakash [21], the source term on the right side of the above three equations is due to the presence of solid, and μ is the dynamic viscosity, θ is the volume fraction of liquid, and Am is the mixture region's consecutive number; it can also be considered porous media permeability. The value of Am is introduced to be smaller than 0.0001 to avoid division by zero, and the value of Am is fixed at 10^5, as Chenzhen et al. [22] concluded for Rubitherm 42.

$\theta(T)$ can be defined as:

$$\theta(T) = \begin{cases} 0T < \left(T_m - {\triangle T}/{2}\right) \\ \frac{T - T_m + {\triangle T}/{2S}}{\triangle T}\left(T_m - \frac{\triangle T}{2}\right) \leq T \leq \left(T_m + \frac{\triangle T}{2}\right) \\ 1T > \left(T_m + \frac{\triangle T}{2}\right) \end{cases} \quad (12)$$

Two separate energy equations are employed for PCM and Nickle foam under non-thermal equilibrium conditions. The energy equation for PCM:

$$\varepsilon\rho_p C_{pf}\frac{\partial T_f}{\partial t}+\varepsilon\rho_p C_{pf}\left(u\frac{\partial T_P}{\partial x}+v\frac{\partial T_p}{\partial x}+w\frac{\partial T_p}{\partial z}\right)=k_p\left(\frac{\partial^2 T_p}{\partial x}+\frac{\partial^2 T_p}{\partial y}+\frac{\partial^2 T_p}{\partial z}\right)+h_{sf}A_{sf}(T_s-T_P) \quad (13)$$

The energy equation for metal foam:

$$(1-\varepsilon)\rho_s c_{ps}\frac{\partial T_s}{\partial t}=k_s\left(\frac{\partial^2 Ts}{\partial x}+\frac{\partial^2 Ts}{\partial y}+\frac{\partial^2 Ts}{\partial z}\right)-h_{ps}a_{ps}\left(T_s-T_p\right) \quad (14)$$

The coefficient of interstitial heat transfer between PCM and metal foam is represented by h_{ps}. The Zukauskas expression [23] was used to calculate it.

$$h_{ps}=0.76Re_d^{0.4}Pr^{0.37}\frac{k_p}{k_d},\quad 1\le Re_d\le 40 \quad (15)$$

For metal foam, permeability and the inertial coefficient is calculated using Calmidi's model[7]

Permeability: $K=0.00073d_p^2(1-\varepsilon)^{-0.224}\left(\frac{d_f}{d_p}\right)^{-1.11}$ (16)

Inertial coefficient: $C=0.00212d_p^2(1-\varepsilon)^{-0.132}\left(\frac{d_f}{d_p}\right)^{-1.63}$ (17)

The specific area calculation is carried out using the formula [24]:

$$a_{PS}=\frac{3\pi d_f\left(1-e^{-\left(\left(\frac{1-\varepsilon}{0.004}\right)\right)}\right)}{\left(0.59d_p\right)^2} \quad (18)$$

Where, d_p is the pore diameter and d_r is the equivalent diameter of the metal foam fibers.

The effective thermal conductivity of PCM and metal foam is calculated using the formula [25]:

$k_{Pe}=k_{eff}|k_s=0\ ,\ \ k_{Se}=k_{eff}|k_f=0$

$$k_{eff}=\frac{1}{\sqrt{2(M_A+M_B+M_C+M_D)}} \quad (19)$$

$$M_A=\frac{4\xi}{\left(2e^2+\pi\xi(1-e)\right)k_s+(4-2e^2-\pi\xi)k_f} \quad (20)$$

$$M_B=\frac{(e-2\xi)}{(e-2\xi)e^2k_s+(2e-4\xi-(e-2\xi)e^2)k_f} \quad (21)$$

$$M_c=\frac{\left(\sqrt{2}-2e\right)^2}{2\pi\xi^2\left(1-2\sqrt{2}e\right)k_s+2\left(\sqrt{2}-2e-\pi\xi^2\left(1-2\sqrt{2}e\right)\right)k_f} \quad (22)$$

$$M_D=\frac{2e}{e^2k_s+(4-e^2)k_f} \quad (23)$$

Where,

$$\xi = \sqrt{\frac{\sqrt{2}\left(2-\left(\frac{5}{8}\right)e^{3}\sqrt{2}-2\varepsilon\right)}{\pi\left(3-4\sqrt{2}e-e\right)}}, e = 0.339 \quad (24)$$

For PCM, ε=1, $k_{Pe}=k_{Se}$ *and* $h_{PS}a_{PS}(T_S-T_P)=0$.

The numerical model is solved using FEA with COMSOL Multiphysics. The solver was selected automatically by COMSOL, and necessary modifications were made.

Mesh Study:

Four different element sizes were used to investigate the sensitivity of mesh size, as seen in the image. The melt fraction changed similarly for all mesh sizes, with a minor variance, between 0 and 1 percent. The solution is more exact when the mesh size is small. A mesh size of 260103 elements is used in this study.

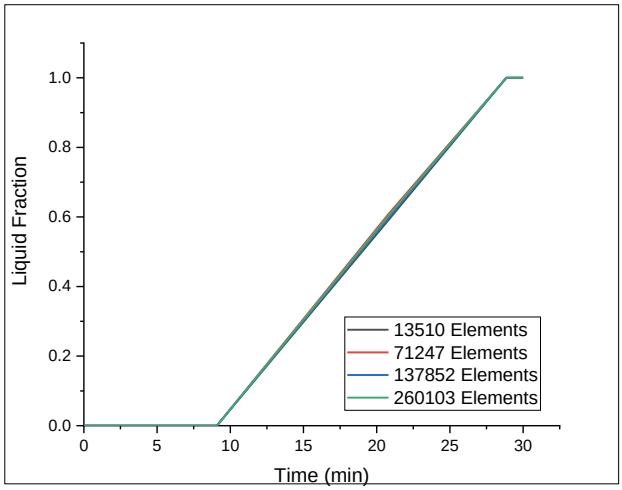

Figure 2. Effect Of Mesh Size Variation on Melt Fraction

Results and Discussion:

Battery Pack performance under different cooling modes at different C-Rates:

Natural air convection, pure PCM, and nickel paraffin composite were utilised to test the battery pack's performance. The coefficient of heat transfer was calculated to be 8.75 W/m^2.K [26]. The metal foam with ε=0.97 and 30 PPI was chosen for this simulation. The surface temperature of all six cells is recorded but only cell 3 is presented here. The temperature profile for 0.5C is shown in fig 3(a). In case of natural convection, the temperature reaches 37°C during 0.5C discharge.

The temperature in case of Pure PCM and Nickle Paraffin composites reaches 35°C and 33°C, respectively. Because convective air has a low heat transfer coefficient, the temperature of the cell surface more in natural convection.

For 1.5C discharge, simulation is repeated, and the temperature profile is sown in fig 3(b). In the case of Nickle Paraffin composite, the cell surface temperature rises to 40°C, which is 25% lower than that of natural convection. Pure PCM achieves a cell surface temperature of 44°C, which is 19% lower than natural convection. Due to the low heat conductivity of PCM, the cell surface temperature rises dramatically. In the case of PCM, the temperature of the PCM near the cell rises faster than the rest of the pack, and phase change begins to reach the melting threshold. There are two elements to the temperature profile: sensible heat and latent heat. Nickle paraffin composite provides an enhanced thermal conductivity for better heat dissipation within the pack hence reaching a lower value of cell surface temperature.

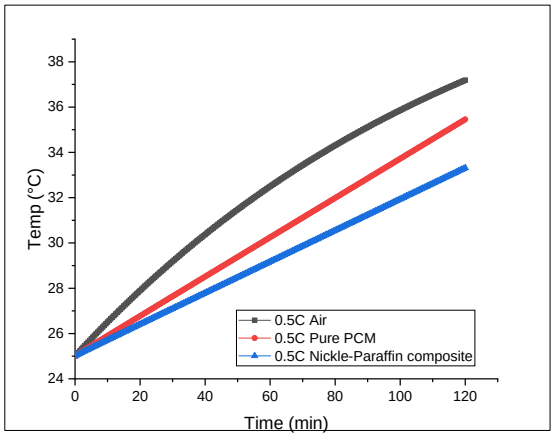

(a)

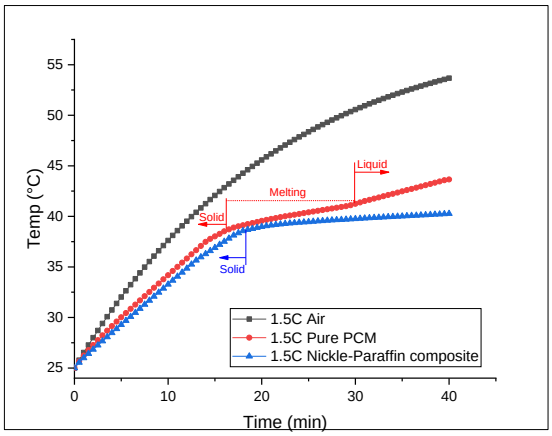

(b)

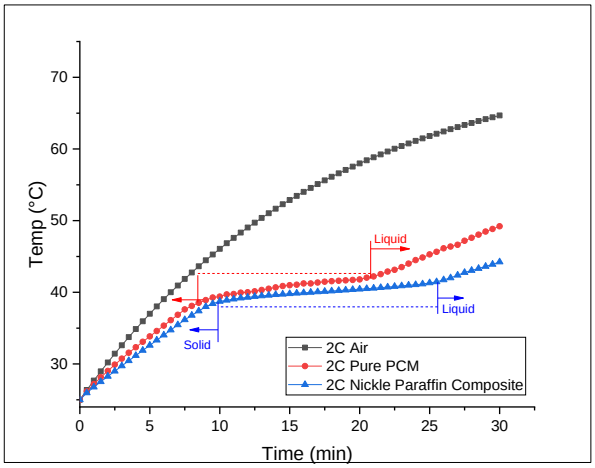

(c)

Fig 3. Temperature profiles under different cooling modes (a) 0.5C (b) 1.5C (c) 2C

Figure 3 depicts the temperature profile for a 2C discharge (c). The cell surface temperature of the Nickle Paraffin composite reaches 44 °C, which is 31% lower than that of natural air. The cell temperature hits 49 °C when pure PCM is utilized as a cooling medium, which is 23 % lower than natural convection. These temperature differences across all three discharge rates indicate that the Nickle Paraffin composite is the optimum cooling medium for Li-ion battery thermal management.

Uniformity of Temperature:

A battery pack of 6s arrangement is under investigation. For the battery pack's longevity, it's critical to achieve a uniform temperature distribution. Figure 4 (a) shows the temperature differential between cell 1 and cell 3 for a 2C discharge using Pure PCM and Nickle Paraffin composite cooling modes. Under Pure PCM cooling mode, a temperature differential of 2.5 °C is recorded between cells 1 and 3. The same difference is reduced to 1.5 °C in the case of Nickle Paraffin composite. This variation is observed due to the melt fraction difference of the Pure PCM and Nickle Paraffin composite. The melt fraction comparison in both cases is shown in fig 4(b). Pure PCM starts melting earlier than Nickle Paraffin composite, according to the results. Metal foam does, in fact, improve thermal conductivity and so increase the rate of heat transport. The PCM's limited thermal conductivity reduces heat spread, resulting in a greater temperature in cell 3.

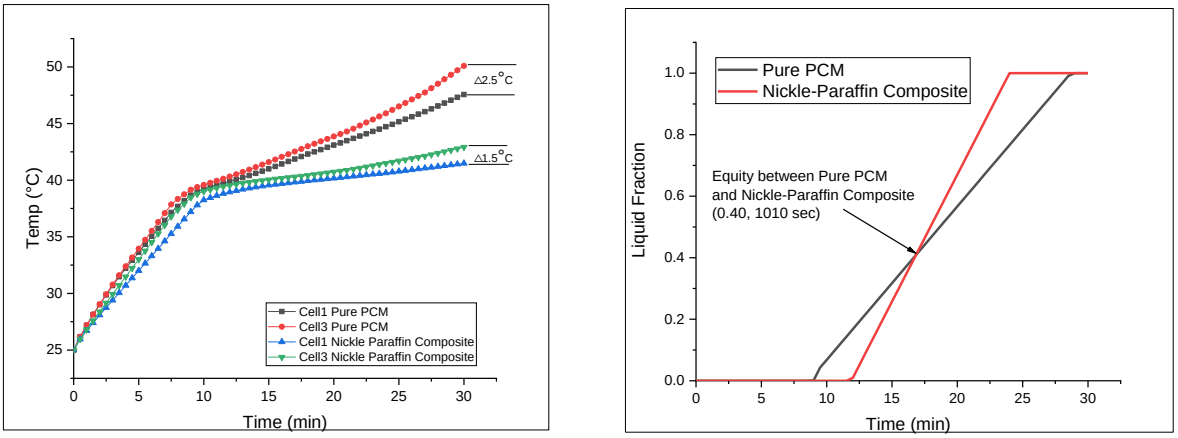

(a) (b)

Figure 4. (a) Temperature Comparison of cell 1 and cell 3 under 2c Discharge (b) Melt Fraction Comparison under 2c Discharge

Fig 5 shows the surface temperature profile under 2C discharge for Pure PCM and Nickle Paraffin composite. The temperature profile can show the difference in surface temperature between cells. The cell in the battery pack's middle gets a higher temperature than the cells on the sides. In the case of the Nickle-Paraffin composite, the temperature gradient is reduced.

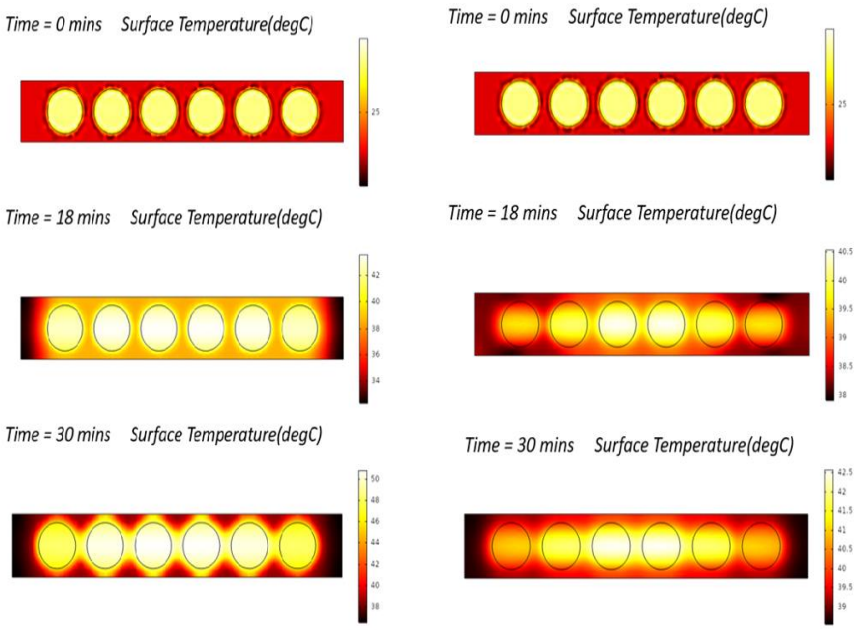

(a) (b)

Fig 5. Temperature profile under 2C discharge rate (a) Pure PCM (b) Nickle Paraffin Composite

Capacity Fading:

Figure 6 depicts the capacity fading of a single cell at various discharge rates. The current research relies on the integration of electrochemical and heat transfer models. The capacity fading of the cell is unaffected by the battery pack's temperature behavior. As a result, all cooling modes show the same pattern at varying discharge rates.

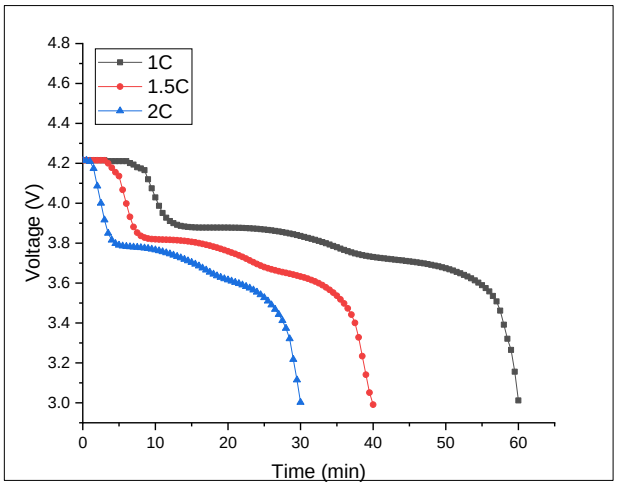

Figure 6. Voltage drop under different C-Rates

Validation of the results:

The numerical model's results were compared to the experimental data from Abid et al. [18] to validate the model. Figure 7 depicts the percentage inaccuracy within a 3-percentage-point range. The error range for natural air convection is only 1%, while the error range for Pure PCM and Metal foam is 2% and 3%, respectively, which is negligible. Overall, the current numerical findings generated are in good agreement with the experimental data, indicating that the model is credible and logical.

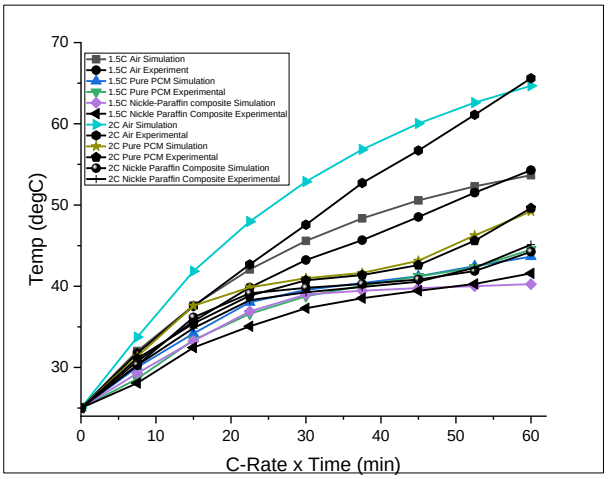

Figure 7. Comparison between Numerical and Experimental study

Conclusion:

The present numerical model validates the experimental study for Li-ion batteries using the electrochemical coupling technique in COMSOL Multiphysics. At 0.5C discharge rate, a very less temperature difference is observed in all three cooling techniques due to temperature gradient and low heat production. The results indicates that for 1.5C discharge rate, temperature reaches 40.2°C with Nickle-Paraffin composite, which is 25% less than that of natural air and 8% less than Pure PCM. For 2C discharge rate, temperature reaches 44.2°C with Nickle-Paraffin composite, which is 31% less than that of natural air and 10% less than Pure PCM. The effectivity of Nickle-Paraffin composite increases with the increase in C-Rate due to high temperature gradient. Metal foam also plays a vital role in decreasing thermal resistance and distributing the heat hence keeping the battery surface at less temperature. The effect of temperature on capacity fading cannot be concluded using the current modelling technique.

Acknowledgement:

We acknowledge Mr. Yousif Muhammad for providing COMSOL Multiphysics software license from the Technical University of Denmark.

Nomenclature:

k	thermal conductivity $\left[\frac{W}{mK}\right]$
h_{ps}	Co-efficient of interstitial heat transfer
K	permeability (m^2)
T	temperature (°C)
t	time (s)
c	Li-ion concentration of $\left(\frac{mol}{m^3}\right)$
L	length (μm)
D	diffusion coefficient $\left(\frac{m^2}{s}\right)$
r	solid particle radius (μm)
ρ	density (kg/m^3)
θ	volume fraction
ε	porosity
a_{PS}	specific area
σ	solid phase conductivity
ε_s	solid phase volume fraction
κ_i	reaction rate co-efficient
ε_e	electrolyte phase volume fraction
μ	dynamic viscosity
t^0	transfer number of electrolyte

[1] G. Jiang, J. Huang, M. Liu, and M. Cao, “Experiment and simulation of thermal management for a tube-shell Li-ion battery pack with composite phase change material,” *Appl. Therm. Eng.*, vol. 120, pp. 1–9, Jun. 2017, doi: 10.1016/j.applthermaleng.2017.03.107.

[2] M.-S. Wu, K. H. Liu, Y.-Y. Wang, and C.-C. Wan, “Heat dissipation design for lithium-ion batteries,” *J. Power Sources*, vol. 109, no. 1, pp. 160–166, Jun. 2002, doi: 10.1016/S0378-

7753(02)00048-4.

[3] P. R. Tete, M. M. Gupta, and S. S. Joshi, “Developments in battery thermal management systems for electric vehicles : A technical review State of Power,” *J. Energy Storage*, vol. 35, no. December 2020, p. 102255, 2021, doi: 10.1016/j.est.2021.102255.

[4] A. Lazrak, J.-F. Fourmigué, and J.-F. Robin, “An innovative practical battery thermal management system based on phase change materials: Numerical and experimental investigations,” *Appl. Therm. Eng.*, vol. 128, pp. 20–32, Jan. 2018, doi: 10.1016/j.applthermaleng.2017.08.172.

[5] F. Samimi, A. Babapoor, M. Azizi, and G. Karimi, “Thermal management analysis of a Li-ion battery cell using phase change material loaded with carbon fibers,” *Energy*, vol. 96, pp. 355–371, Feb. 2016, doi: 10.1016/j.energy.2015.12.064.

[6] Mohamed Moussa El Idi, Mustapha Karkri, “Characterization of the thermal behavior of Li-ion batteries with a view to optimal passive management,” IEEE International Telecommunications Energy Conference (INTELEC), 2018 doi: https://doi.org/10.25855/SFT2020-148.

[7] M. Moussa *et al.*, “Caractérisation du comportement thermique des batteries Li- ion en vue d ’ une gestion optimale passive composite : Experimental and numerical investigations.” Congrès Annuel de la Société Française de Thermique, 2020 doi: 10.25855/SFT2020-148

[8] M. Malik, I. Dincer, and M. A. Rosen, “Review on use of phase change materials in battery thermal management for electric and hybrid electric vehicles,” Int. J. Energy Res., vol. 40, no. 8, pp. 1011–1031, Jun. 2016, doi: 10.1002/er.3496.

[9] M. Doyle, T. F. Fuller, and J. Newman, “Modeling of Galvanostatic Charge and Discharge of the Lithium/Polymer/Insertion Cell,” *J. Electrochem. Soc.*, vol. 140, no. 6, pp. 1526–1533, Jun. 1993, doi: 10.1149/1.2221597.

[10] B. Mortazavi, H. Yang, F. Mohebbi, G. Cuniberti, and T. Rabczuk, “Graphene or h-BN paraffin composite structures for the thermal management of Li-ion batteries: A multiscale investigation,” Appl. Energy, vol. 202, pp. 323–334, 2017, doi: 10.1016/j.apenergy.2017.05.175.

[11] H. Maleki, S. Al Hallaj, J. R. Selman, R. B. Dinwiddie, and H. Wang, “Thermal Properties of Lithium-Ion Battery and Components,” J. Electrochem., vol. 146, no. 3, pp. 947–954, 1999, doi: 10.1149/1.1391704.

[12] K. Kumaresan, G. Sikha, and R. E. White, “Thermal Model for a Li-Ion Cell,” J. Electrochem., vol. 155, no. 2, p. A164, 2008, doi: 10.1149/1.2817888.

[13] L. Cai and R. E. White, “Mathematical modeling of a lithium-ion battery with thermal effects in COMSOL Inc. Multiphysics (MP) software,” J. Power Sources, vol. 196, no. 14, pp. 5985–5989, Jul. 2011, doi: 10.1016/j.jpowsour.2011.03.017.

[14] D. A. G. Bruggeman, “Berechnung verschiedener physikalischer Konstanten von heterogenen Substanzen. III. Die elastischen Konstanten der quasiisotropen Mischkörper

aus isotropen Substanzen," Ann. Phys., vol. 421, no. 2, pp. 160–178, 1937, doi: 10.1002/andp.19374210205.

[15] S. D. V. S. S. V. Siruvuri and P. R. Budarapu, "Studies on thermal management of Lithium-ion battery pack using water as the cooling fluid," J. Energy Storage, vol. 29, no. August 2019, p. 101377, 2020, doi: 10.1016/j.est.2020.101377.

[16] S. Renganathan, G. Sikha, S. Santhanagopalan, and R. E. White, "Theoretical Analysis of Stresses in a Lithium-Ion Cell," J. Electrochem., vol. 157, no. 2, p. A155, 2010, doi: 10.1149/1.3261809.

[17] G. Sikha, R. E. White, and B. N. Popov, "A Mathematical Model for a Lithium-Ion Battery/Electrochemical Capacitor Hybrid System," J. Electrochem., vol. 152, no. 8, p. A1682, 2005, doi: 10.1149/1.1940749.

[18] A. Hussain, C. Y. Tso, and C. Y. H. Chao, "Experimental investigation of a passive thermal management system for high-powered lithium-ion batteries using nickel foam-paraffin composite," Energy, vol. 115, pp. 209–218, 2016, doi: 10.1016/j.energy.2016.09.008.

[19] V. Paserin, S. Marcuson, J. Shu, and D. S. Wilkinson, "CVD Technique for Inco Nickel Foam Production," Adv. Eng. Mater., vol. 6, no. 6, pp. 454–459, Jun. 2004, doi: 10.1002/adem.200405142.

[20] Z. Qin, C. Ji, Z. Low, S. Dubey, F. Hoong Choo, and F. Duan, "Effect of Fin Location on the Latent Heat Storage: A Numerical Study," Energy Procedia, vol. 143, pp. 320–326, Dec. 2017, doi: 10.1016/j.egypro.2017.12.691.

[21] V. V. R. & P. C., "A Fixed grid numerical modelling methodology for convection diffusion mushy region phase change problems," Int. Jounal Heat Mass Transf., vol. 30, no. 8, pp. 1709–1719, 1978.

[22] C. Ji, Z. Qin, S. Dubey, F. H. Choo, and F. Duan, "Simulation on PCM melting enhancement with double-fin length arrangements in a rectangular enclosure induced by natural convection," Int. J. Heat Mass Transf., vol. 127, pp. 255–265, Dec. 2018, doi: 10.1016/j.ijheatmasstransfer.2018.07.118.

[23] S. B. Beale, "Fluid flow and heat transfer in tube banks.," Foreign Aff., vol. 91, no. 5, pp. 1689–1699, 2012, [Online]. Available: http://hdl.handle.net/10044/1/8103.

[24] W. Q. Li, Z. G. Qu, Y. L. He, and Y. B. Tao, "Experimental study of a passive thermal management system for high-powered lithium-ion batteries using porous metal foam saturated with phase change materials," J. Power Sources, vol. 255, pp. 9–15, Jun. 2014, doi: 10.1016/j.jpowsour.2014.01.006.

[25] K. Boomsma and D. Poulikakos, "On the effective thermal conductivity of a three-dimensionally structured fluid-saturated metal foam," Int. J. Heat Mass Transf., vol. 44, no. 4, pp. 827–836, Feb. 2001, doi: 10.1016/S0017-9310(00)00123-X.

[26] P. Kosky, R. Balmer, W. Keat, and G. Wise, "Mechanical Engineering," in Exploring Engineering, Elsevier, 2021, pp. 317–340.